Accepted paper

J. Cardoso, N. Ben Sedrine, A. Alves, M. A. Martins, M. Belloeil, B. Daudin, D. Nd. Faye, E. Alves, K. Lorenz, A. J. Neves, M. R. Correia and T. Monteiro.

Multiple optical centers in Eu-implanted AlN nanowires for solid state lighting applications. Appl. Phys. Lett. 113, 201905 (2018).

10.1063/1.5048772

This manuscript was accepted by Appl. Phys. Lett. Click here to see the version of record.

Multiple optical centers in Eu-implanted AlN nanowires for solid-state lighting applications

J. Cardoso[1], N. Ben Sedrine[1,*], A. Alves[1], M. A. Martins[2], M. Belloeil[3], B. Daudin[3], D. Nd. Faye[4], E. Alves[4], K. Lorenz[4,5], A. J. Neves[1], M. R. Correia[1] and T. Monteiro[1]

[1] Departamento de Física e I3N, Universidade de Aveiro, Campus Universitário de Santiago, 3810-193 Aveiro, Portugal
[2] Departamento de Física e CICECO, Universidade de Aveiro, 3810-193 Aveiro, Portugal
[3] Univ. Grenoble Alpes, CEA/CNRS Group, "Nanophysique et Semiconducteurs", F-38000 Grenoble, France
[4] IPFN, Instituto Superior Técnico, Campus Tecnológico e Nuclear, Estrada Nacional 10, P-2695-066 Bobadela LRS, Portugal
[5] Instituto de Engenharia de Sistemas de Computadores - Microsystems and Nanotechnology (INESC-MN), Rua Alves Redol, 1000-029 Lisboa, Portugal

A detailed spectroscopic analysis of Eu^{3+} implanted and annealed AlN nanowires (NW) grown by plasma-assisted molecular beam epitaxy is presented by using micro-Raman, temperature-dependent steady-state photoluminescence and time-resolved photoluminescence. Two different annealing temperatures (1000 ºC and 1200 ºC) were used. Such annealing conditions achieved a recovery of the original AlN crystalline structure as confirmed by Raman analysis. For both samples, the red Eu^{3+} intra-$4f^6$ luminescence was demonstrated, where the $^5D_0 \rightarrow {}^7F_2$ transition at 624 nm is the most intense. Two well-resolved Eu optically active centers were observed in the present AlN NW and designated as Eu1 and Eu2, due to their similar spectral shape when compared to those observed in GaN layers [L. Bodiou, A. Braud, J.L. Doualan, R. Moncorgé, K. Lorenz, and E. Alves, Optical Materials **28**, 780 (2006); I.S. Roqan, K.P. O'Donnell, R.W. Martin, P.R. Edwards, S.F. Song, A. Vantomme, K. Lorenz, E. Alves, and M. Boćkowski, Physical Review B **81**, 085209 (2010)]. Their behavior was found to depend on the annealing temperature. Photoluminescence studies reveal that at 14 K, Eu2 is dominant for the lower annealing temperature, while Eu1 is dominant for the highest annealing temperature. Moreover, at room temperature, Eu1 center was found to be the dominant for both samples. Indeed, the luminescence intensity of the $^5D_0 \rightarrow {}^7F_2$ transition exhibits a lower thermal quenching for the samples annealed at the highest temperature (~80 % for the sample annealed at 1200 ºC, and ~50 % for the sample annealed at 1000 ºC) boosting their potential use as efficient red emitters.

***Author to whom correspondence should be addressed: nbensedrine@ua.pt, bsnebiha@yahoo.fr**

One of the major issues related to the use of group-III nitrides in optoelectronic devices, such as visible light emitting devices (LEDs), is their low efficiency in the green/red spectral region[1]. Such disadvantage hinders the development of powerful monolithic white LEDs and full-color displays based on III-N semiconductors. A possible solution to surpass this barrier involves controlled doping strategies able to enhance the green/red light emission. One of the established approaches consists of the intentional insertion of rare-earth (RE) ions in III-N hosts, taking advantage of their narrow atomic-like transitions at characteristic wavelengths[2,3]. The range of the intra-$4f^n$ emission lines from RE ions in the trivalent charge state (3+) covers the entire visible spectrum, allowing to tune the emission to the desired color through the proper choice of the ion. In III-nitride semiconductors, the RE ions tend to occupy cation substitutional (or near-substitutional) sites, promoting the achievement of the trivalent charge state[4]. In the last decade, this approach has been widely investigated (particularly in GaN) and the first LED

This manuscript was accepted by Appl. Phys. Lett. Click here to see the version of record.

based on a GaN:Eu^{3+} active layer was achieved in 2009 by Eu *in-situ* doping during growth[5]. Since then, some work was also performed on Eu implanted directly in diode structures[6,7].

AlN is a direct wide-bandgap semiconductor (bandgap of 6.2 eV at room temperature[8]) with a high transparency in the visible region. Furthermore, AlN is chemically inert and has robust physical properties. It is an interesting host for the incorporation and optical activation of RE ions due to an expected lower thermal luminescence quenching when compared with narrow bandgap semiconductors[9]. Despite these interesting properties, scarce works have been performed yet on RE-doped AlN, with reported emission lines corresponding to RE^{3+} ions such as Eu, Pr, Tm and Tb[2,10,11].

The luminescence from trivalent RE ions involves intra-4f^n transitions when introduced in a host. In the case of the free ion, these transitions are parity forbidden by electric dipole according to the Laporte selection rules. When introduced in a crystal, the crystal-field perturbation causes the admixture of 4*f*-states with different parity states, which leads to a relaxation of the selection rules following the Judd-Ofelt theory[12,13]. As a result, the intra-4*f* transitions become partially allowed. The crystal-field perturbation also contributes to the splitting of the energy levels in several Stark levels, depending on their multiplicity and the symmetry of the local field. Trivalent europium ions (Eu^{3+}) are known to emit efficiently in the orange/red spectral region, due to their intra-4f^6 transitions between the crystal-field split energy levels of the ^5D_J and ^7F_J manifolds[14,15].

The choice of low-dimensional structures, such as nanowires (NW), has gained a special interest as building blocks for future optoelectronic devices. Indeed, NW can provide an increased efficiency of light emitting devices due to the absence/reduction of extended defects which behave as non-radiative recombination centers. Furthermore, it is possible to grow NW on cheaper and even on highly mismatched substrates, such as silicon substrates which are well-established in the actual micro technologies. Moreover, a larger surface to volume ratio favoring the accommodation of doping-induced strain makes them favorable with respect to their 2D layer counterparts and a higher light extraction is also expected from these nanostructures[16,17].

In this work, we explore the capability of Eu-implanted and annealed AlN NW to be a potential approach for the development of efficient red-emitters at the nanoscale. The study is focused on the behavior of the most intense intra-4f^6 transition $^5D_0 \rightarrow {}^7F_2$ and the identification of two main optically active Eu centers in the AlN host.

The studied AlN NW were grown at ~865 ºC by plasma-assisted molecular beam epitaxy (PA-MBE) on silicon (Si) (111) oriented substrate. A thin (3 - 4 nm) AlN buffer layer was deposited, followed by intentionally Si-doped GaN NW base structure, and AlN NW on top. More details can be found in Ref. [18].

The incorporation of Eu in the AlN NW was realized by ion implantation at room temperature (RT) using 300 keV ions, with a fluence of 1×10^{14} Eu.cm^{-2}. The implantation was performed with a tilt angle of 45° with respect to the *c*-axis and the samples were rotated during the implantation, using the geometry shown in Fig. 1 (a). With this geometry, Eu is expected to be implanted only in the AlN-section of the NW since the bases of the NW will be shadowed. The rotation allows a homogeneous distribution of Eu defects avoiding bending of the NW due to implantation-induced strain, even if some ions enter through the side facets[19]. According to Monte Carlo simulations using the SRIM 2013 code[20], the projected range is 54 nm leading to a doped layer thickness of about 100 nm with a maximum Eu concentration of 3×10^{19} at.cm^{-2}. Note that SRIM does not take into account the three-dimensional geometry of the NW, nevertheless, due to the strong coalescence of NW close to the surface, the thin layer model gives good estimates of the Eu distribution.

Post-implantation rapid thermal annealing (RTA) was carried out at two temperatures: 1000 °C (sample N-1000) and 1200 °C (sample N-1200), during 30 seconds under N_2 flow.

RTA at 1000 °C achieved efficient optical activation of implanted rare-earth ions in GaN NW[21]. At higher temperatures, GaN is expected to dissociate; a process which is aggravated in NW due to the large surface area to volume ratio. Nevertheless, AlN-capping of GaN thin films was shown to efficiently protect GaN from dissociation[21,22]. Therefore, a second temperature of 1200 °C was tested, since typically increasing the annealing temperature yields higher Eu luminescence intensity[21,23]. Furthermore, these annealing conditions were reported for rare-earth implanted AlGaN thin films[4].

Structural properties of the as-grown, implanted and annealed samples were investigated by scanning electron microscopy (SEM) using a high resolution Schottky emission (SE), Hitachi model SU-70 equipped with detectors for secondary and backscattered electrons. Fig. 1 also shows representative SEM images of the vertically aligned NW of the as-grown and N-1200 samples in cross-section (b) and (c) and top-view (d) and (e), respectively. The SEM images of the as-implanted (as-imp) and N-1000 samples can be found in Figs. S1 (a) and (b), respectively, in the supplementary material. The NW length is of ~2 µm, composed of ~0.5 µm of AlN (red arrow) and ~1.5 µm of GaN:Si (green arrow). In all samples, the NW diameters vary along the axis from a few tens of nanometers at the base to about 100-200 nanometers at the tip, exhibiting partial coalescence of the NW, likely due to the bundling of the NW as was recently discussed by Kaganer *et al*.[24]. In addition, the non-zero lateral growth rate of the AlN NW, due to the limited diffusion of Al along the side walls towards the top[18], combined to the high NW density are favoring the coalescence in their upper part. As can be seen from the representative SEM cross-section images of as-grown [Fig. 1 (b)] and N-1200 [Fig. 1 (c)] samples, no noticeable differences are recorded, indicating that no severe damage of the GaN/AlN NW structure after implantation/post-implantation annealing occurs. In addition, it is important to notice that, far from the cutting samples' zone, SEM top-view images exhibit a morphology that is not affected neither by implantation, nor by post-implantation annealing [Fig. 1 (e), Figs. S1 (a) and (b) in the supplementary material].

RT micro-Raman measurements were performed using a Horiba Jobin-Yvon micro-Raman HR800 spectrometer in the backscattering geometry, $z(x, \cdot)\bar{z}$, to minimize the signal from the substrate. The 442 nm line of a HeCd laser (Kimmon IK Series) was used for excitation and the beam was focused with a ×100 magnification objective (NA=0.9, f=0.1 cm). In addition to N-1000 and N-1200 samples, as-grown and as-imp samples were also studied using micro-Raman spectroscopy. Photoluminescence (PL) measurements were realized using the 325 nm excitation wavelength (~3.8 eV) of a HeCd laser (power density less than 0.6 W.cm^{-2}), corresponding to an energy above and below the GaN and AlN bandgap energy, respectively. The samples were mounted in the cold tip of a closed-cycle helium cryostat, which permits to control the temperature from 14 K to RT. The PL signal was measured through a dispersive system SPEX 1704 monochromator (1 m, 1200 grooves.mm^{-1}) coupled to a cooled Hamamatsu R928 photomultiplier tube. RT time-resolved photoluminescence (TRPL) spectra were acquired in a Fluorolog-3 Horiba scientific modular system with a pulsed Xe lamp as excitation source coupled to a monochromator (excitation wavelength of 325 nm). The measurements were carried out using the front face acquisition geometry, and the presented spectra were corrected to the spectral response of the optical components and the Xe lamp. It should be noticed that, due to the higher dimensions of the excitation spot size in comparison to the NW average size, several hundreds of nanowires were simultaneously probed in the following optical study.

Fig. 2 (a) shows the Raman spectra of the AlN NW samples recorded using the 442 nm excitation. The calculated phonon density of states (DOS) for GaN and AlN are also included for comparison[25]. The Raman response of the as-grown sample exhibits the phonon modes allowed in the used dispersion geometry: E_2^H (GaN) at 568 cm^{-1}, and E_2^H (AlN) at 655 cm^{-1}. For relaxed samples, these phonon frequencies are reported to be 567.6 cm^{-1} and 657.4 cm^{-1},

respectively[25]. Therefore, the phonon frequencies obtained for as-grown AlN NW, suggest that E_2^H (GaN) is nearly relaxed, while the E_2^H (AlN) is redshifted by ~2 cm^{-1}. This redshift indicates the presence of a tensile strain in the present as-grown AlN NW. Furthermore, forbidden phonon modes in this dispersion geometry are also present in the Raman response of the as-grown AlN NW: E_1^{TO} (GaN) and A_1^{TO} (AlN), indicating a slight misorientation of the *c*-axis relatively to the laser beam incidence. After implantation (sample as-imp), the Raman response shows the activation of the AlN phonon DOS induced by the damage created in the crystal. Fig. 2 (b) summarizes the evolution of the E_2^H (AlN) phonon frequency and full-width at half maximum (FWHM) versus the implantation and annealing temperature. These values correspond to the best-fit model of the phonon modes using Lorentzian functions. After implantation, the tensile strain is enhanced and FWHM increases by a factor of ~2. After annealing, a gradual relaxation of the strain is obtained and the recovery of the original AlN crystalline structure is observed. The recovery is better achieved for the annealing temperature of 1200 ºC for which the E_2^H (AlN) FWHM is equal to the one of the as-grown sample. We have found that the E_2^H (GaN) phonon mode is not affected neither by the implantation nor by the annealing at 1000 ºC, indicating that the Eu-implantation only occurs in the AlN structure, as will be further discussed. After annealing at 1200 ºC, the Raman signal of the E_2^H (GaN) phonon mode is not observed in some regions of the sample, as shown for N-1200 (point B) in Fig. S2 in the supplementary material. We attribute the reduction/absence of the vibrational mode to an increase of the optical absorption along the structure, due to the generated optical defects by the highest annealing temperature. Although no noticeable structural changes were identified in the probed regions by cross-sectional SEM images, we cannot discard the contribution of a possible GaN dissociation, since it was demonstrated that GaN starts to dissociate during RTA above ~ 1000 ºC, while AlN is stable at higher temperatures[21,22].

PL spectra of the Eu implanted and annealed samples, measured at 14 K, are presented in Fig. 3. Vertical dashed lines correspond to the Eu^{3+} intra-$4f^6$ transitions $^5D_0 \rightarrow {}^7F_J$ (J = 1, 2, 3); their peak positions and assignments are also listed in Table I. The values reported by Gruber *et al*. for Eu in-*situ* doped AlN single crystals are also included for comparison. In this work, the obtained $^5D_0 \rightarrow {}^7F_{1,2,3}$ transitions for Eu-implanted AlN NW are in good agreement with the ones reported by Gruber *et al*.[26]. For both samples N-1000 and N-1200, the $^5D_0 \rightarrow {}^7F_2$ transition (also called hypersensitive transition) centered at ~624 nm is the most intense. This value is in good agreement with the reported one for Eu-implanted AlN layers[10,27] and nanostructures[28]. Thus, it is possible to confirm the optical activation of the Eu ions in the AlN NW after RTA annealing used in this work. It is noticeable that, under the used experimental excitation conditions, the $^5D_0 \rightarrow {}^7F_0$ transition (~590 nm in Ref.[26]) is not observed.

Fig. 4 represents a magnification around the $^5D_0 \rightarrow {}^7F_2$ transition at 14 K and RT for samples N-1000 and N-1200. A closer inspection of the hypersensitive transition reveals that the intra-ionic transition is composed of more than three well-resolved emission lines (FWHM of ~0.4 nm for each line) predicted by the local crystal-field symmetry[26], which suggests the presence of more than one optically active Eu center. The obtained spectral shape and the relative intensity of the transitions between the different Stark levels vary as expected for two different optical Eu centers, hereafter designated as Eu1 and Eu2 due to the similarity of their spectral shapes when compared to the well-stablished Eu centers in GaN hosts[29–31]. The most prominent lines occurring at 623.44 nm and 624.44 nm (for the sample N-1000) are attributed to the Eu2 and Eu1 centers, respectively (as indicated by vertical dashed lines in Fig. 4 and summarized in Table I). Since the two centers are observed for both annealing temperatures, it is expected that Eu occupies the same lattice sites in the N-1000 and N-1200 samples. In GaN:Eu, these centers have been attributed to Eu^{3+} ions in substitutional cation sites either isolated, Eu2, or perturbed by different nearby defects, Eu1, namely nitrogen or cation vacancies[31,32]. Despite the similar spectral shape, the excitation mechanisms of the Eu centers

This manuscript was accepted by Appl. Phys. Lett. Click here to see the version of record.

in GaN and AlN are different. For instance, both Eu1 and Eu2 in AlN NW are excited with below AlN bandgap energy, whereas in GaN:Eu, only Eu1 is observed for below GaN bandgap excitation[33].

The behavior of Eu centers in AlN depends on the annealing temperature since the spectral shape and the relative intensity of the transitions between the different Stark levels vary. Annealing at 1000 ºC induces the contribution to PL from the two centers, Eu1 and Eu2, while annealing at 1200 ºC causes an apparent decrease of the Eu2 contribution, resulting in a preponderant Eu1 center. It is worth noticing that an opposite behavior of Eu1 and Eu2 was reported in GaN:Eu layers and nanostructures, being expected an increase of the Eu2 contribution for higher annealing temperatures[29,30,34]. It is well-stablished that Eu2 center is the most relevant under current injection conditions in GaN hosts (for above bandgap excitation)[32]. Thus, if we assume that the Eu2 center in AlN NW has the same characteristics as in GaN, annealing at a temperature of 1000 ºC would be enough for future developments of red-emitting devices.

At RT, in addition to the decrease of the intra-$4f^6$ luminescence intensity, a slight broadening of the spectral lines associated to the transitions between the different Stark levels is observed. Furthermore, a higher contribution from Eu1 center to the overall RT luminescence is obtained regardless of the annealing temperature. This result suggests that Eu1 and Eu2 centers have different thermal quenching mechanisms.

Fig. 5 demonstrates the different thermal quenching obtained from the temperature dependence of the $^5D_0 \rightarrow {}^7F_2$ PL integrated intensity for N-1000 and N-1200 samples. Due to competitive thermally activated non-radiative processes, the global luminescence intensity decreases gradually with increasing temperature for sample N-1000, reaching at RT ~50 % of the 14 K luminescence intensity. At RT, ~80 % of the 14 K PL intensity is still observed for N-1200. Such temperature behavior of the dominant lines in the hypersensitive transition further corroborates our assumption that more than one optically active Eu center exists in the studied Eu-implanted and annealed AlN NW. For the sample N-1200, the luminescence intensity decreases faster until 120 K then slightly increases for higher temperatures, indicating the presence of a thermally activated population mechanism. Since this behavior is only observed for the sample N-1200, we exclude the possibility of energy-transfer between the two Eu centers if the thermal behavior is exclusively related to such process. Therefore, it is likely that the thermal population is due to additional defects generated by the highest annealing temperature.

The comparison of the ratio between the intra-$4f^6$ luminescence intensity at RT versus 14 K in GaN NW (~50 %)[34,35] and N-1200 sample (~80 %) reveals that the introduction of Eu ions in the wider bandgap material leads to a lower thermal quenching, indicating that AlN:Eu NW can play an important role in the development of efficient red-emitters based on group-III nitrides.

Besides the steady-state photoluminescence, an attempt to discriminate the Eu1 and Eu2 centers was carried out by RT TRPL. Using a sample window of 0.2 ms, a value of ~0.4 ms was estimated for the lifetime of the $^5D_0 \rightarrow {}^7F_2$ transition centroid (Fig. S3 in the supplementary material) for both samples.

In summary, Eu-implanted and annealed AlN NW were studied by micro-Raman and PL spectroscopy. It was found that the damage caused in the AlN crystalline structure of the NW by Eu implantation is completely recovered by rapid thermal annealing. Independently of the annealing temperature, the NW exhibit Eu^{3+} emission, confirming the optical activation of Eu ions in the AlN host. The analysis of the most intense $^5D_0 \rightarrow {}^7F_2$ transition evidences that two distinct Eu centers (Eu1 and Eu2), being excited below the AlN bandgap, can be identified. Their behavior is found to depend on the annealing temperature: Eu2 is dominant for the

annealing temperature of 1000 ºC, while Eu1 is dominant for the annealing temperature of 1200 ºC. Furthermore, the PL temperature dependence demonstrates a predominance of Eu1 center at RT for both samples. The sample N-1200 exhibits a ratio between the luminescence intensity at RT versus 14 K of ~80% which is higher than the ~50% obtained for the sample N-1000, as well as the one in GaN hosts. Although the Eu^{3+} emission from N-1200 sample exhibits a higher thermal stability, the RTA at 1000 ºC is enough to activate the europium. Therefore, the possibility of tuning the relative concentration of different optically active Eu centers via the annealing temperature may become important when optimizing the excitation through current injection in future light emitting devices.

See supplementary material for additional scanning electron microscopy images of as-imp and N-1000 samples, Raman spectrum obtained in a different region (designated as point B) of the N-1200 sample, and room temperature time-resolved photoluminescence for samples N-1000 and N-1200.

Acknowledgments

The authors acknowledge financial support from FEDER funds through the POR Lisboa, COMPETE 2020 Programme and National Funds through FCT - Portuguese Foundation for Science and Technology under the projects UID/CTM/50025/2013, POCI-01-0145-FEDER-028011 & LISBOA-01-0145-FEDER-029666 and the bilateral program Pessoa. The authors also acknowledge Ana Violeta Girão, from CICECO laboratory, for her support with SEM measurements.

References

[1] M. Auf Der Maur, A. Pecchia, G. Penazzi, W. Rodrigues, and A. Di Carlo, Physical Review Letters **116**, 027401 (2016).

[2] H.J. Lozykowski and W.M. Jadwisienczak, Physica Status Solidi (b) **244**, 2109 (2007).

[3] K.P. O'Donnell and B. Hourahine, The European Physical Journal Applied Physics **36**, 91 (2006).

[4] M. Fialho, J. Rodrigues, S. Magalhães, M.R. Correia, T. Monteiro, K. Lorenz, and E. Alves, Semiconductor Science and Technology **31**, 035026 (2016).

[5] A. Nishikawa, T. Kawasaki, N. Furukawa, Y. Terai, and Y. Fujiwara, Applied Physics Express **2**, 071004 (2009).

[6] D.N. Faye, M. Fialho, S. Magalhães, E. Alves, N. Ben Sedrine, J. Rodrigues, M.R. Correia, T. Monteiro, M. Boćkowski, V. Hoffmann, M. Weyers, and K. Lorenz, Nuclear Instruments and Methods in Physics Research B **379**, 251 (2016).

[7] N. Ben Sedrine, J. Rodrigues, J. Cardoso, D.N. Faye, M. Fialho, S. Magalhães, A.F. Martins, A.J. Neves, E. Alves, M. Boćkowski, V. Hoffmann, M. Weyers, K. Lorenz, M.R. Correia, and T. Monteiro, Surface and Coatings Technology (2018), DOI: 10.1016/j.surfcoat.2018.02.004.

[8] Q. Yan, A. Janotti, M. Scheffler, and C.G. Van De Walle, Applied Physics Letters **105**, 111104 (2014).

[9] P.N. Favennec, H. L'Haridon, M. Salvi, D. Moutonnet, and Y. Le Guillou, Electronics Letters **25**, 718 (1989).

[10] H.J. Lozykowski, W.M. Jadwisienczak, A. Bensaoula, and O. Monteiro, Microelectronics Journal **36**, 453 (2005).

[11] W.M. Jadwisienczak, H.J. Lozykowski, I. Berishev, A. Bensaoula, and I.G. Brown, Journal of Applied Physics **89**, 4384 (2001).

[12] B.R. Judd, Phys. Rev. **127**, 750 (1962).

[13] G.S. Ofelt, The Journal of Chemical Physics **37**, 511 (1962).

[14] M. Peres, A. Cruz, M.J. Soares, A.J. Neves, T. Monteiro, K. Lorenz, and E. Alves, Superlattices and Microstructures **40**, 537 (2006).

[15] K. Binnemans, Coordination Chemistry Reviews **295**, 1 (2015).

[16] S. Zhao, H.P.T. Nguyen, M.G. Kibria, and Z. Mi, Progress in Quantum Electronics **44**, 14 (2015).

[17] A. Henneghien, G. Tourbot, B. Daudin, O. Lartigue, Y. Désières, and J.-M. Gérard, Optics Express **19**, 527 (2011).

[18] M. Belloeil, B. Gayral, and B. Daudin, Nano Letters **16**, 960 (2016).

[19] C. Ronning, C. Borschel, S. Geburt, and R. Niepelt, Materials Science and Engineering R **70**, 30 (2010).

[20] J.F. Ziegler, J.P. Biersack, and M.D. Ziegler, *SRIM: The Stopping and Range of Ions in Matter* (SRIM Co., Chester (Md.), 2008) , http://www.srim.org (last accessed July 2018).

[21] K. Lorenz, U. Wahl, E. Alves, S. Dalmasso, R.W. Martin, K.P. O'Donnell, S. Ruffenach, and O. Briot, Applied Physics Letters **85**, 2712 (2004).

[22] E. Nogales, R.W. Martin, K.P.O. Donnell, K. Lorenz, E. Alves, S. Ruffenach, O. Briot, E. Nogales, R.W. Martin, and K.P.O. Donnell, Applied Physics Letters **88**, 031902 (2006).

[23] K. Lorenz, S.M.C. Miranda, E. Alves, I.S. Roqan, K.P. O'Donnell, and M. Boćkowski, in *Proceedings of SPIE* (2012), p. 82620C–82620C–6.

[24] V.M. Kaganer, S. Fernández-Garrido, P. Dogan, K.K. Sabelfeld, and O. Brandt, Nano Letters **16**, 3717 (2016).

[25] V.Y. Davydov, Y.E. Kitaev, I.N. Goncharuk, A.N. Smirnov, J. Graul, O. Semchinova, D. Uffmann, M.B. Smirnov, A.P. Mirgorodsky, and R.A. Evarestov, Physical Review B **58**, 12899 (1998).

[26] J.B. Gruber, U. Vetter, T. Taniguchi, G.W. Burdick, H. Hofsäss, S. Chandra, and D.K. Sardar, Journal of Applied Physics **110**, 023104 (2011).

[27] K. Wang, K.P. O'Donnell, B. Hourahine, R.W. Martin, I.M. Watson, K. Lorenz, and E. Alves, Physical Review B - Condensed Matter and Materials Physics **80**, 125206 (2009).

[28] S. Magalhães, M. Peres, V. Fellmann, B. Daudin, A.J. Neves, E. Alves, T. Monteiro, and K.

Lorenz, Journal of Applied Physics **108**, 084306 (2010).

[29] L. Bodiou, A. Oussif, A. Braud, J.L. Doualan, R. Moncorgé, K. Lorenz, and E. Alves, Optical Materials **28**, 780 (2006).

[30] L. Bodiou, A. Braud, J.L. Doualan, R. Moncorgé, J.H. Park, C. Munasinghe, A.J. Steckl, K. Lorenz, E. Alves, and B. Daudin, Journal of Applied Physics **105**, 043104 (2009).

[31] I.S. Roqan, K.P. O'Donnell, R.W. Martin, P.R. Edwards, S.F. Song, A. Vantomme, K. Lorenz, E. Alves, and M. Bońkowski, Physical Review B **81**, 085209 (2010).

[32] B. Mitchell, N. Hernandez, D. Lee, A. Koizumi, Y. Fujiwara, and V. Dierolf, Physical Review B **96**, 064308 (2017).

[33] K. Wang, R.W. Martin, K.P. O'Donnell, V. Katchkanov, E. Nogales, K. Lorenz, E. Alves, S. Ruffenach, and O. Briot, Applied Physics Letters **87**, 112107 (2005).

[34] J. Rodrigues, M.F. Leitão, J.F.C. Carreira, N. Ben Sedrine, N.F. Santos, M. Felizardo, T. Auzelle, B. Daudin, E. Alves, A.J. Neves, M.R. Correia, F.M. Costa, K. Lorenz, and T. Monteiro, The Journal of Physical Chemistry C **120**, 6907 (2016).

[35] J. Rodrigues, M.F. Leitão, J.F.C. Carreira, N. Ben Sedrine, N.F. Santos, M. Felizardo, T. Auzelle, B. Daudin, E. Alves, A.J. Neves, M.R. Correia, F.M. Costa, K. Lorenz, and T. Monteiro, The Journal of Physical Chemistry C **119**, 17954 (2015).

Table I

Transition	Peak	Assignment	Sample N-1000 14 K (± 0.05 nm)	Sample N-1200 14 K (± 0.05 nm)	AlN layers 11 K [Gruber *et al.* (2011)[26]]
$^5D_0 \rightarrow {}^7F_1$	P1		602.39	602.30	602.49
	P2		604.34	604.15	604.35
	P3		611.39	611.15	
$^5D_0 \rightarrow {}^7F_2$	Q1	Eu2	623.44	623.40	
	Q2	Eu1/Eu2	623.94	623.90	623.95
	Q3	Eu1	624.44	624.23	624.49
	Q4	Eu1/Eu2	626.59	626.35	
	Q5	Eu1/Eu2	627.69	627.80	
	Q6	Eu1/Eu2	635.79	635.95	635.79
$^5D_0 \rightarrow {}^7F_3$	R1		664.04	663.45	664.03
	R2		665.84	665.80	665.74
	R3		667.29	666.95	667.33
	R4		667.94	667.30	

Table I: Eu^{3+} intra-$4f^6$ transitions observed in the AlN NW and their assignments. Reported values obtained for Eu-implanted AlN layers by Gruber *et al.*[26] are included for comparison.

Figures

Fig. 1: (a) Schematic of the NW structure showing the Eu implantation geometry performed with a tilt angle of 45° with respect to the *c*-axis. Representative SEM images of the AlN as-grown and N-1200 samples: cross-section (b) and (c), and top-view (d) and (e), respectively. In (b) and (c), red arrow: AlN; green arrow: GaN:Si.

Fig. 2: (a) RT normalized Raman spectra of the AlN samples using laser excitation of 442 nm. The spectra were normalized to the maxima of the E_2^H (AlN) phonon mode. The calculated phonon density of states DOS function for GaN and AlN are included for comparison[25]. (b) Frequency and FWHM evolution of the E_2^H (AlN) phonon mode with the Eu-implantation and annealing treatments.

Fig. 3: High-resolution 14K PL spectra of the Eu implanted and annealed samples. Vertical dashed lines correspond to the $^5D_0 \rightarrow {}^7F_{1,2,3}$ transitions; peak positions are also indicated in table I.

Fig. 4: High-resolution PL spectra around the most intense $^5D_0 \rightarrow {}^7F_2$ transition of the Eu implanted and annealed samples, acquired at 14K and RT. Eu2 and Eu1 centers are indicated by vertical dashed lines.

Fig. 5: Temperature dependence of the normalized integrated PL intensity around the most intense $^5D_0 \rightarrow {}^7F_2$ transition of the Eu implanted and annealed samples. Dots and squares: experimental data; full lines: tendency lines (guide for the eyes).

This manuscript was accepted by Appl. Phys. Lett. Click here to see the version of record.

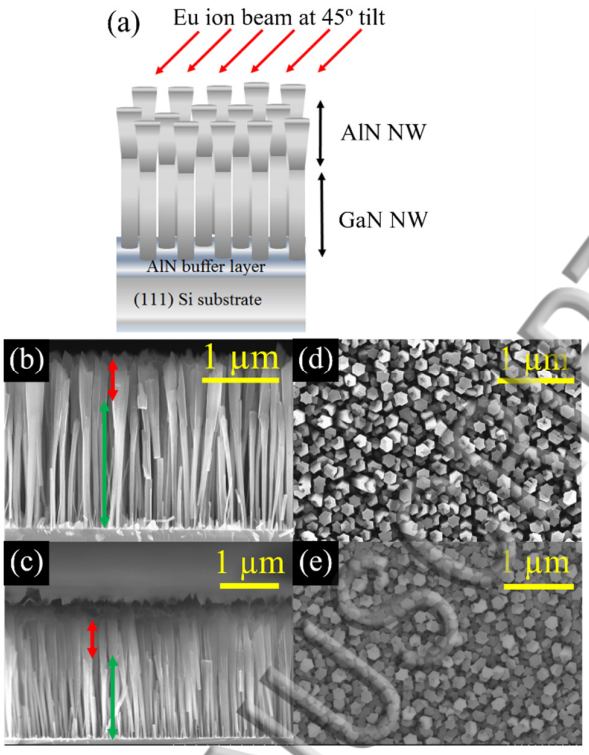

Fig. 1

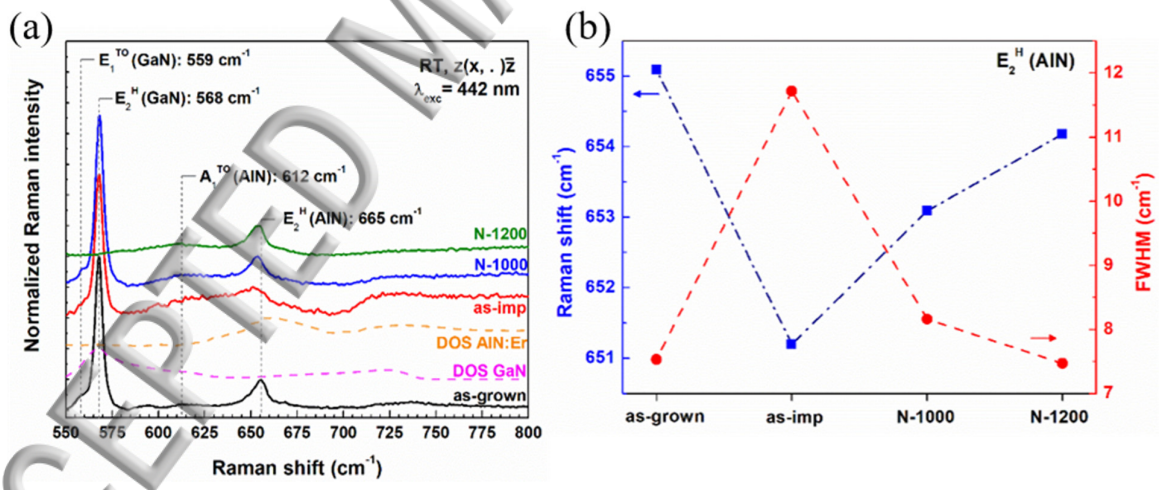

Fig. 2

This manuscript was accepted by Appl. Phys. Lett. Click here to see the version of record.

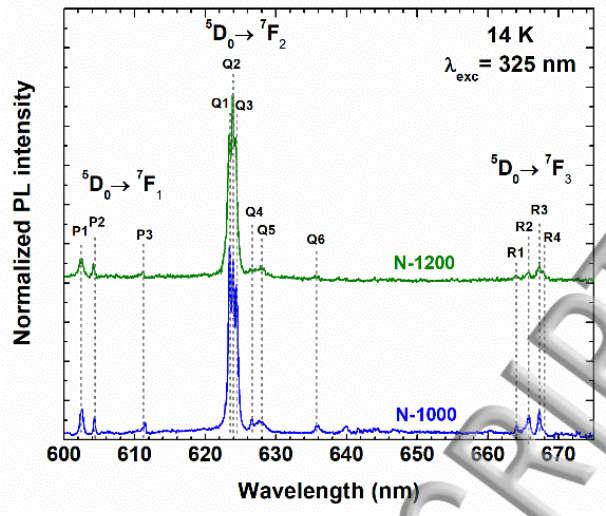

Fig. 3

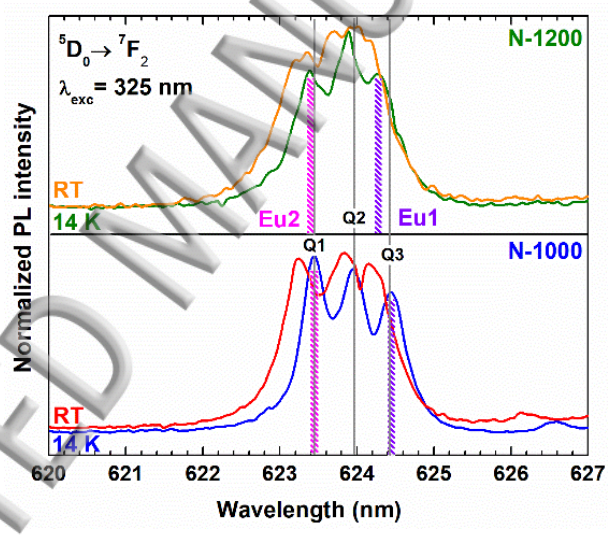

Fig. 4

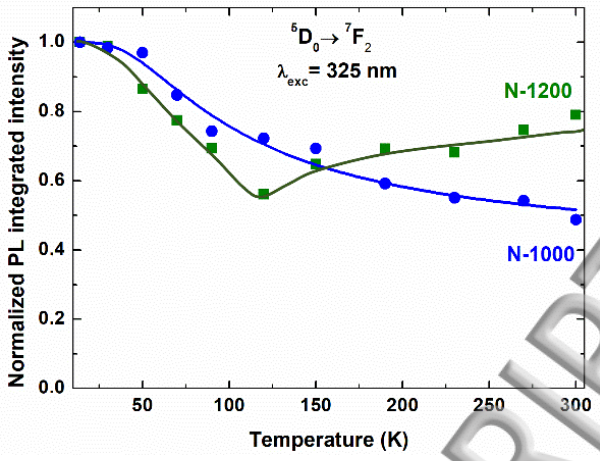

Fig. 5

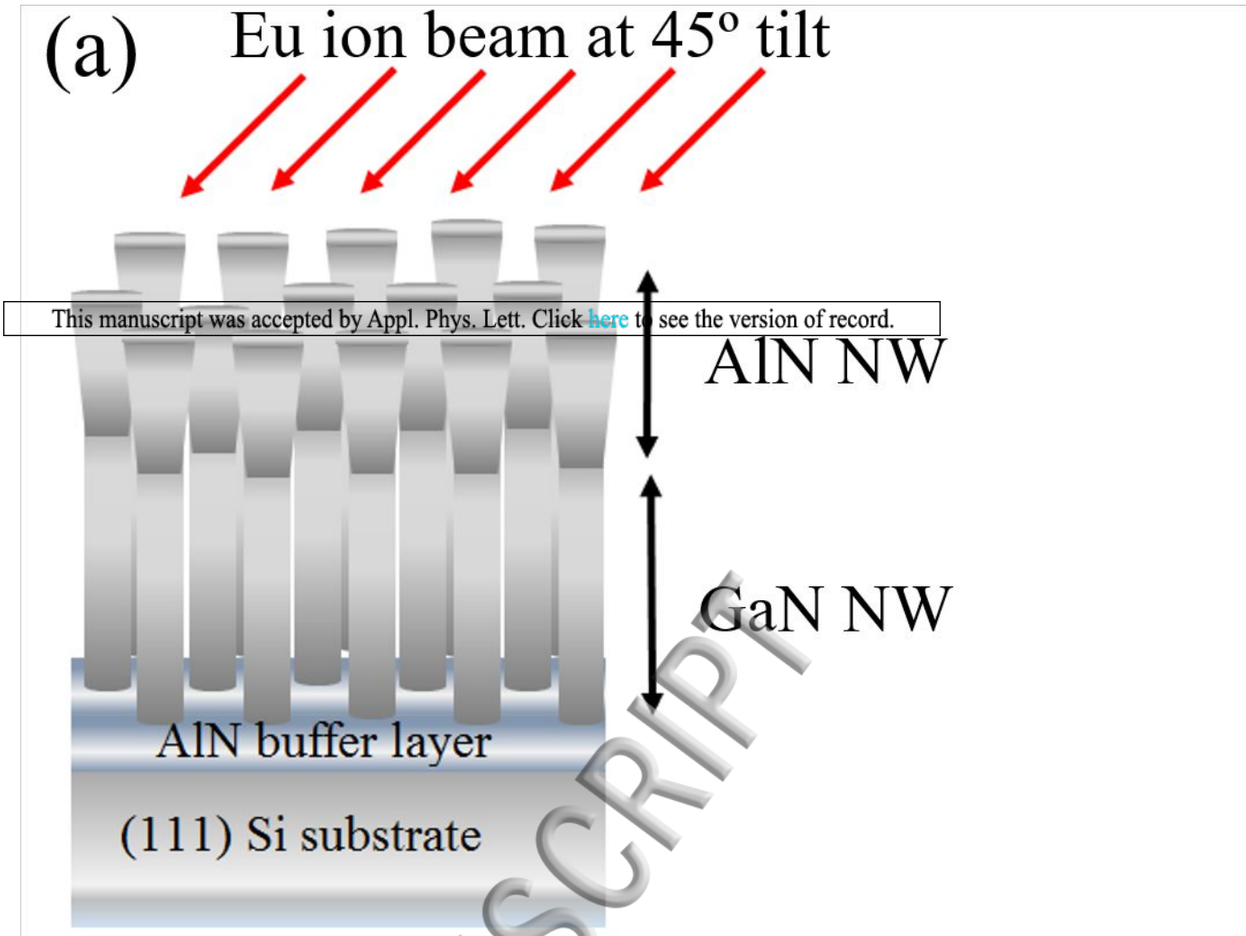

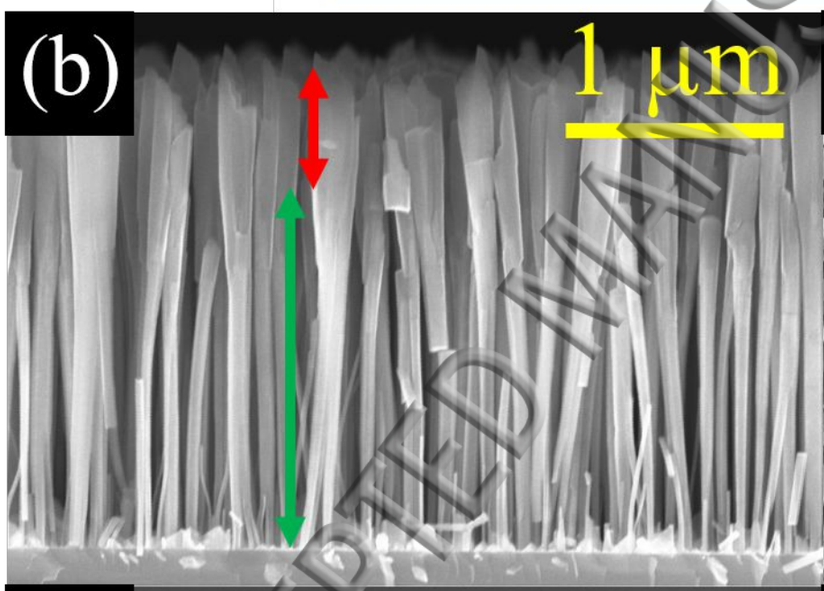

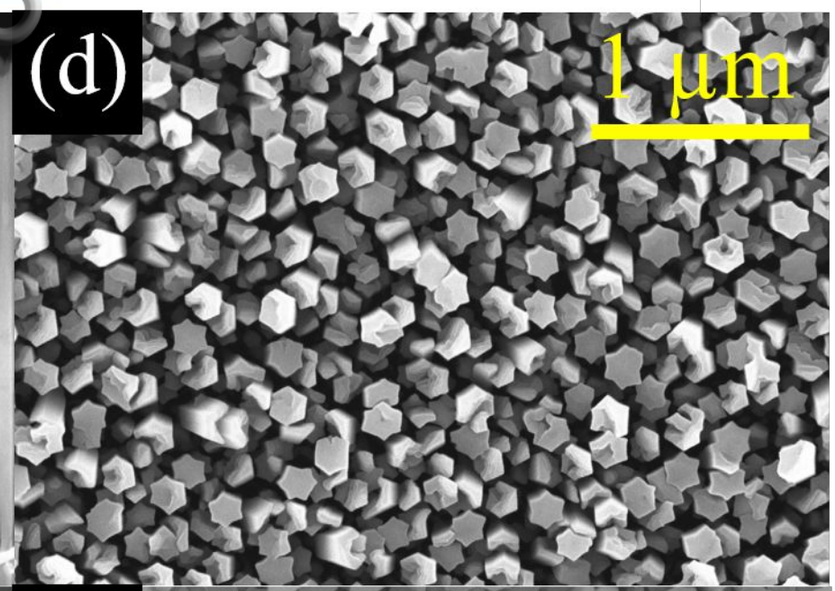

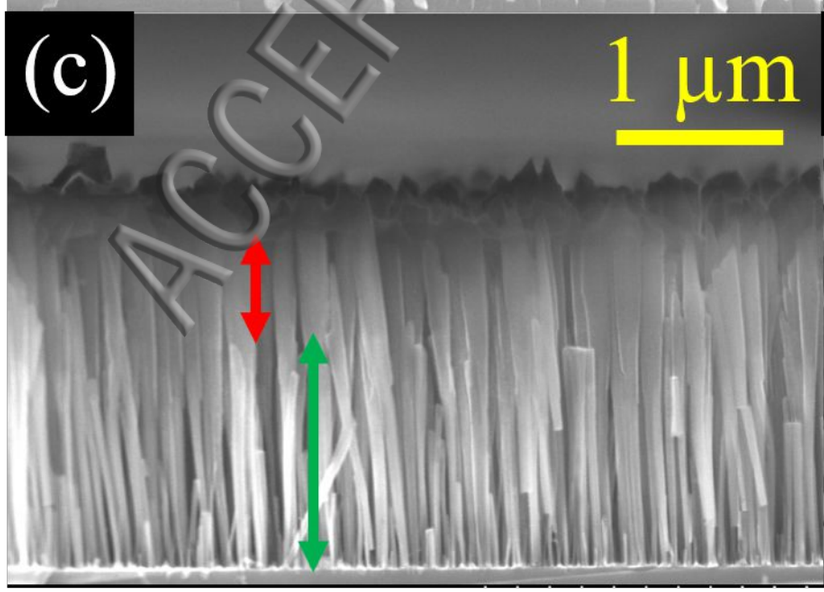

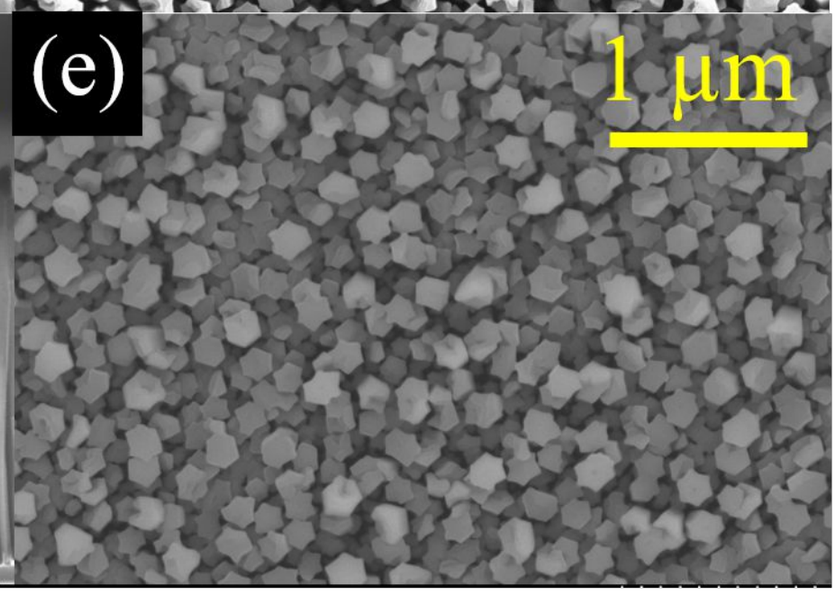

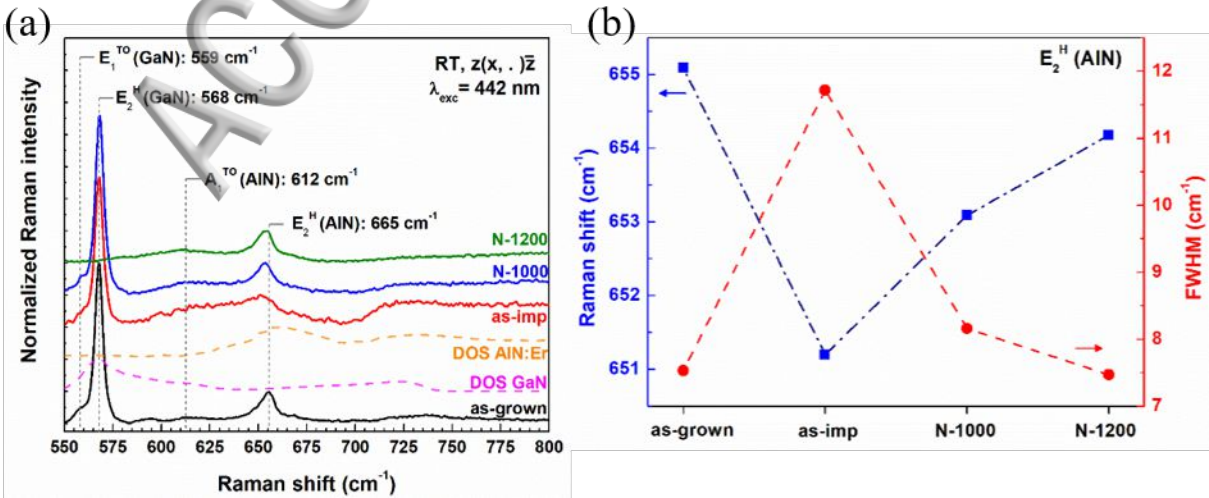
(a)
E_1^{TO} (GaN): 559 cm^{-1}
E_2^H (GaN): 568 cm^{-1}
A_1^{TO} (AlN): 612 cm^{-1}
E_2^H (AlN): 665 cm^{-1}
RT, z(x, .)z̄
λ_{exc} = 442 nm
N-1200
N-1000
as-imp
DOS AlN:Er
DOS GaN
as-grown
Normalized Raman intensity
Raman shift (cm^{-1})
550 575 600 625 650 675 700 725 750 775 800
(b)
E_2^H (AlN)
Raman shift (cm^{-1})
FWHM (cm^{-1})
655 654 653 652 651
12 11 10 9 8 7
as-grown
as-imp
N-1000
N-1200

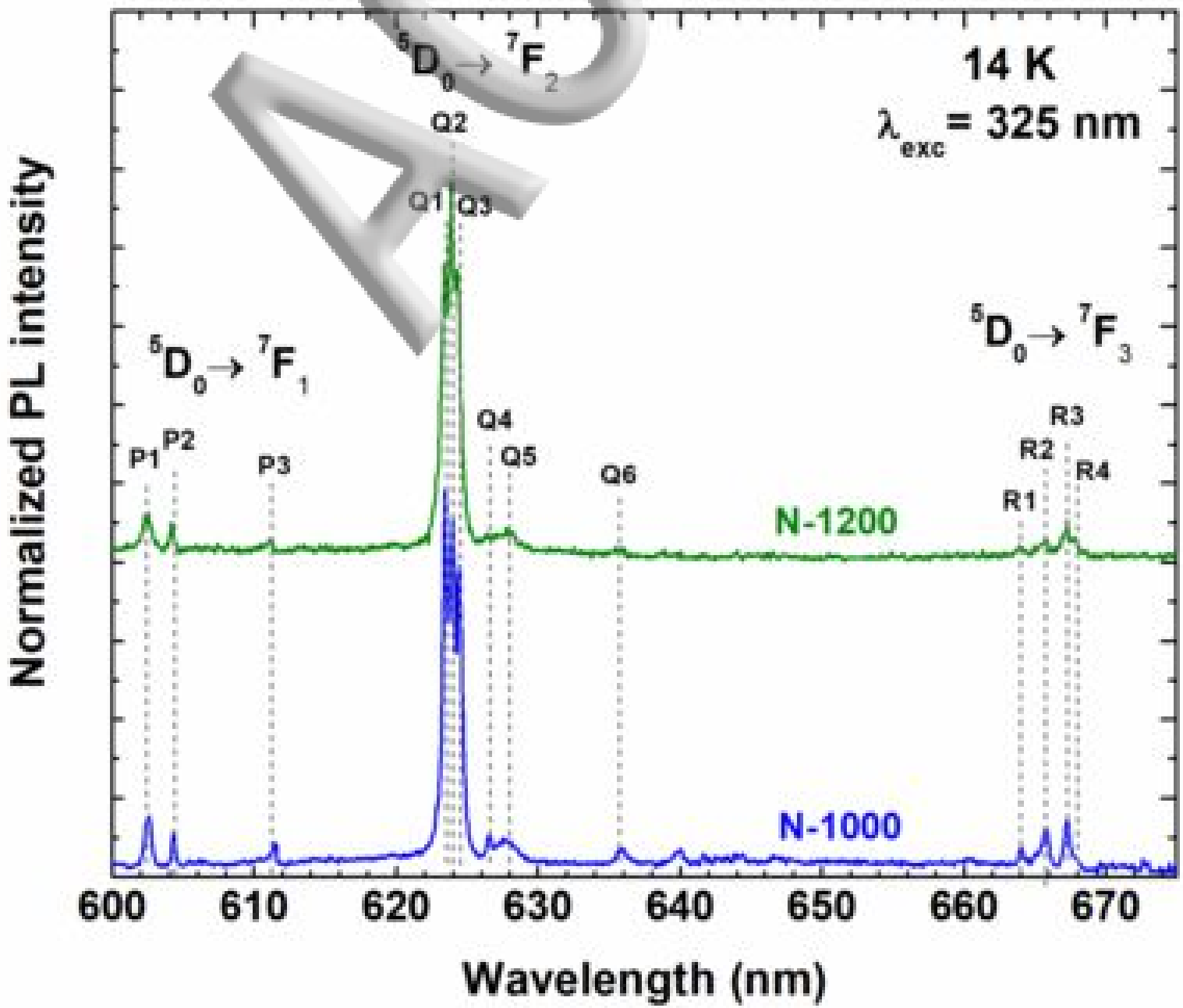
$^5D_0 \rightarrow {}^7F_2$
14 K
λ_{exc} = 325 nm
Q2
Q1
Q3
$^5D_0 \rightarrow {}^7F_1$
$^5D_0 \rightarrow {}^7F_3$
P1
P2
P3
Q4
Q5
Q6
R1
R2
R3
R4
N-1200
N-1000
Normalized PL intensity
600
610
620
630
640
650
660
670
Wavelength (nm)

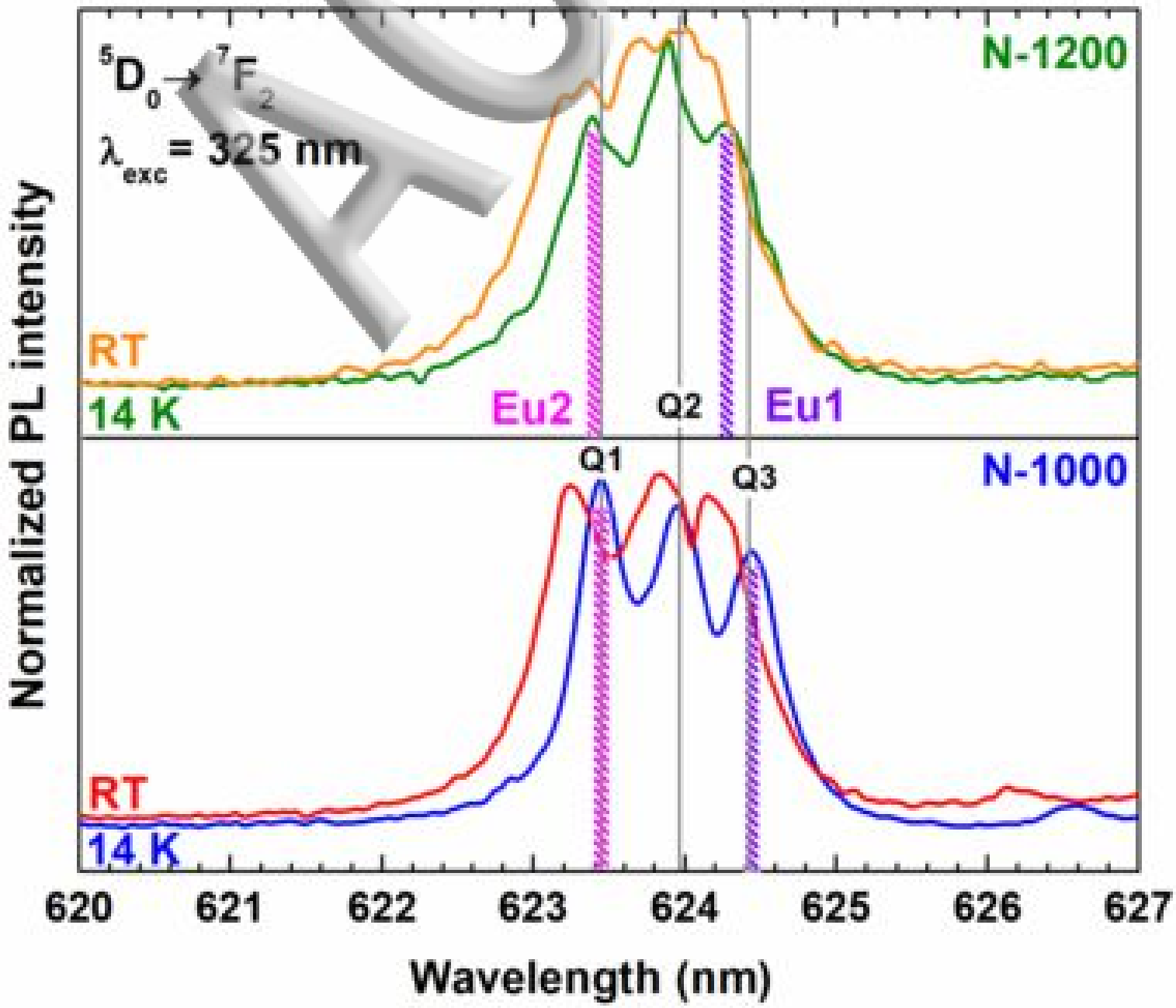
$^5D_0 \rightarrow {}^7F_2$
λ_{exc} = 325 nm
N-1200
RT
14 K
Eu2
Q2
Eu1
Q1
Q3
N-1000
RT
14 K
Normalized PL intensity
620
621
622
623
624
625
626
627
Wavelength (nm)

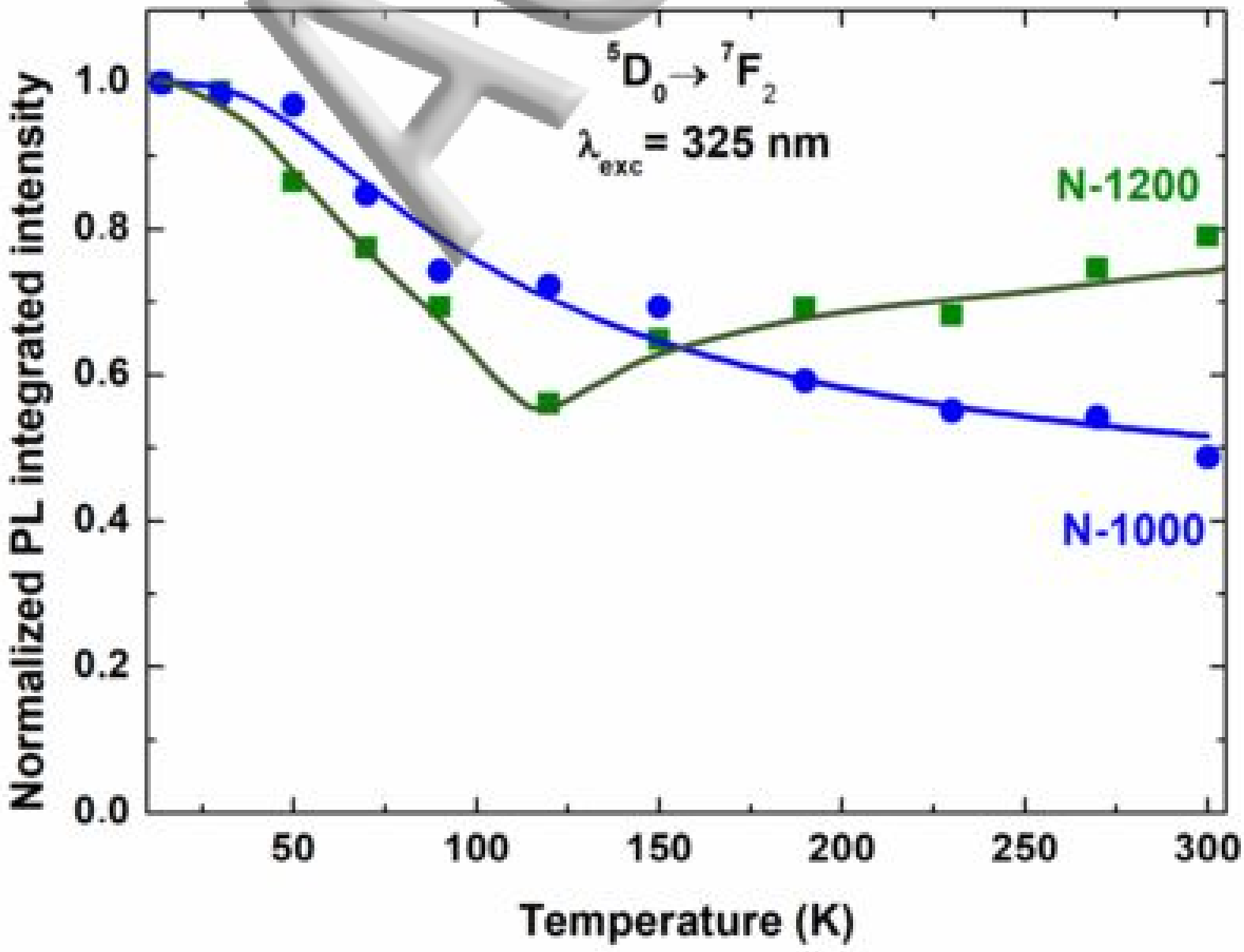
$^5D_0 \rightarrow {}^7F_2$
λ_{exc} = 325 nm
N-1200
N-1000
Normalized PL integrated intensity
1.0
0.8
0.6
0.4
0.2
0.0
50
100
150
200
250
300
Temperature (K)

Supplementary Material:

Multiple optical centers in Eu-implanted AlN nanowires for solid-state lighting applications

J. Cardoso[1], N. Ben Sedrine[1,*], A. Alves[1], M. A. Martins[2], M. Belloeil[3], B. Daudin[3], D. Nd. Faye[4], E. Alves[4], K. Lorenz[4,5], A. J. Neves[1], M. R. Correia[1] and T. Monteiro[1]

[1] Departamento de Física e I3N, Universidade de Aveiro, Campus Universitário de Santiago, 3810-193 Aveiro, Portugal

[2] Departamento de Física & CICECO, Universidade de Aveiro, 3810-193 Aveiro, Portugal

[3] Univ. Grenoble Alpes, CEA/CNRS Group, "Nanophysique et Semiconducteurs", F-38000 Grenoble, France

[4] IPFN, Instituto Superior Técnico, Campus Tecnológico e Nuclear, Estrada Nacional 10, P-2695-066 Bobadela LRS, Portugal

[5] Instituto de Engenharia de Sistemas de Computadores - Microsystems and Nanotechnology (INESC-MN), Rua Alves Redol, 1000-029 Lisboa, Portugal

1. Scanning electron microscopy (SEM):

Top-view SEM images of AlN nanowires (NWs) after implantation with Eu ions (as-imp) and after Eu-implantation and rapid thermal annealing treatment at 1000 °C (N-1000) are shown in Figs. S1 (a) and (b), respectively.

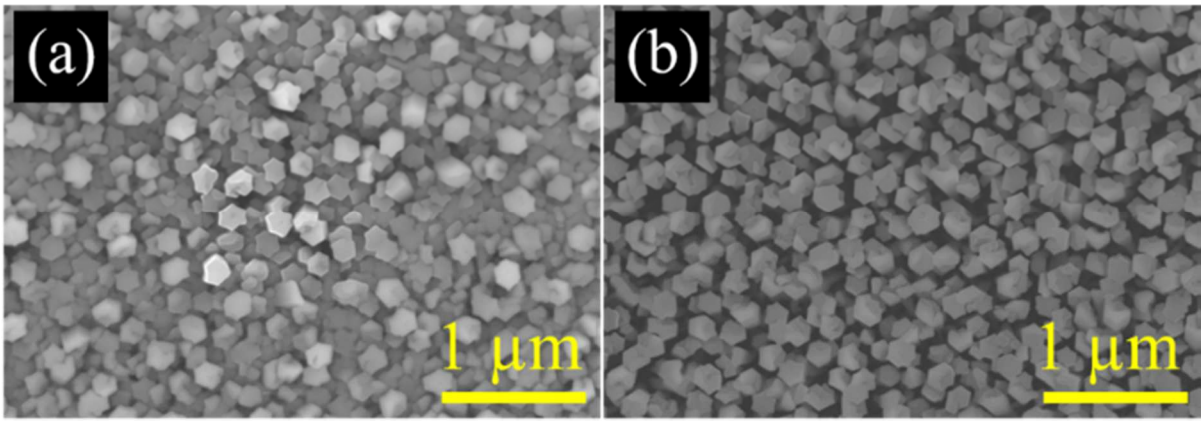

Fig. S1: Top-view SEM images of the AlN NWs as-implanted (a) and N-1000 (b) samples.

2. Raman Spectroscopy:

Fig. S2 shows the comparison of Raman spectra presented in Fig. 2 (a) acquired in the first region [here denoted as point A (pt. A)] with the spectrum obtained in a different region [designated as point B (pt. B)] of the sample implanted and annealed at 1200 °C (N-1200). The presence of the Raman signal from the E_2^H (GaN) mode in this region reveals that sample N-1200 is heterogeneous and two distinct regions can be identified. Additionally, different strain states are observed, either for GaN or AlN phonon modes. Despite these two regions have been identified in sample N-1200, the Raman spectrum of pt. A is representative of a large sample area in which PL measurements were also performed. The same strategy was adopted for the other samples presented in this work (as-grown, as-imp and N-1000).

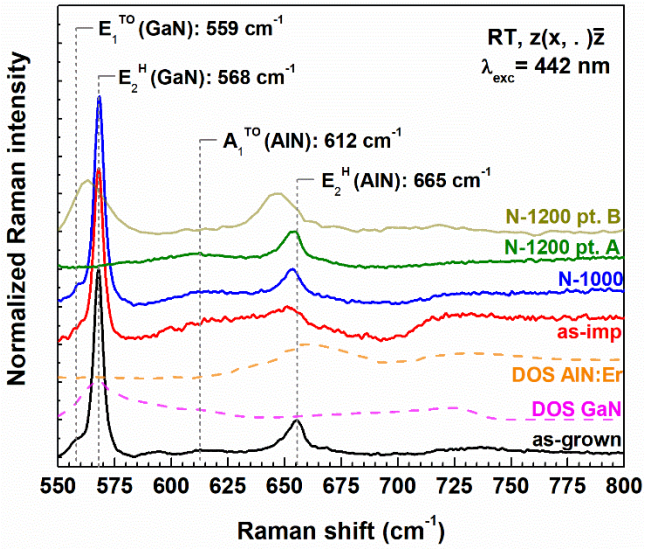

Fig. S2: RT normalized Raman spectra of AlN NW samples using the laser line excitation of 442 nm. The spectra were normalized to the maxima of the E_2^H (AlN) phonon mode. In these spectra, it is possible to look with particular interest for two different points of the sample N-1200, which evidence its heterogeneity. The spectrum in pt. A is representative of a large area of sample N-1200 in which PL measurements were also performed.

3. Room temperature time-resolved photoluminescence (RT TRPL) :

Room temperature time-resolved photoluminescence (RT TRPL) in the intra-4*f* ^{6} range for samples N-1000 and N-1200 using the 325 nm excitation wavelength are shown in Figs. S3 (a) and (b), respectively. Using a sample window of 0.2 ms, a value of ~0.4 ms was estimated for the lifetime of the $^5D_0 \rightarrow {}^7F_2$ transition centroid for both samples.

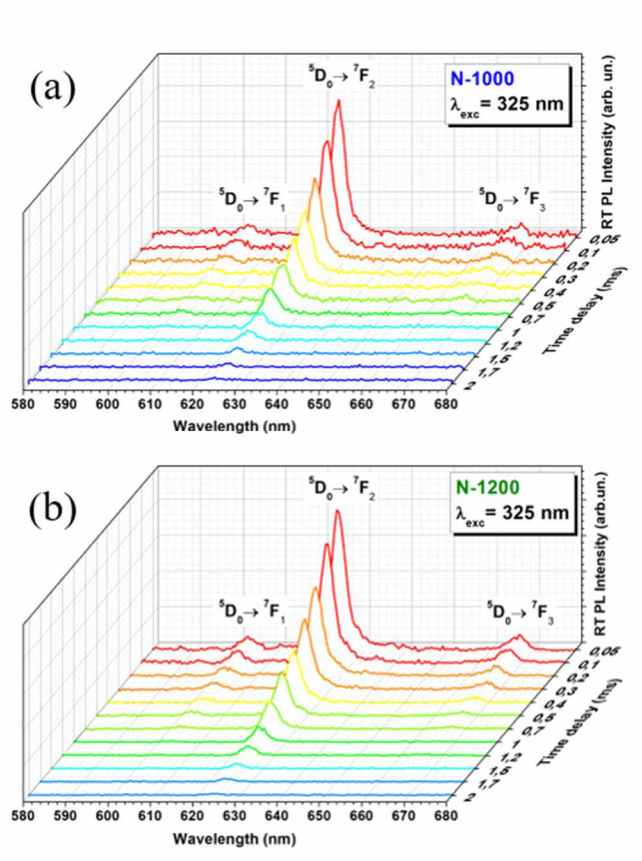

Fig. S3: RT TRPL of samples N-1000 and N-1200 using an excitation wavelength of 325 nm. The most intense emission corresponds to the $^5D_0 \rightarrow {}^7F_2$ transition which intensity vanishes at ~2 ms independently of the annealing temperature.